Optimal heterogeneity of a highly renewable pan-European electricity system

Emil H. Eriksen[a], Tom Brown[b], Martin Greiner[c]

[a]*Department of Physics and Astronomy, Aarhus University, 8000 Aarhus C, Denmark*
[b]*Frankfurt Institute of Advanced Studies (FIAS), Johann Wolfgang Goethe Universität, Ruth-Moufang-Straße 1, 60438 Frankfurt am Main, Germany*
[c]*Department of Engineering, Aarhus University, 8200 Aarhus, Denmark*

Abstract

The resource quality and the temporal generation pattern of variable renewable energy sources vary significantly across Europe. Spatial distributions of renewable assets are explored which exploit this heterogeneity to lower the total system costs for a given level of renewable electricity in Europe. A local search algorithm as well as more intuitive heuristic algorithms are used to find optimal distributions of generation capacities that minimise backup, transmission and renewable capacity costs simultaneously. Using current cost projections, an optimal distribution favours onshore wind in countries bordering the North Sea, which results in average electricity costs that are up to 17% lower than a homogeneous distribution of renewables proportional to each country's mean load. The sensitivities of the results to changing costs of solar generation and different mixes of onshore and offshore wind are also examined.

Keywords: renewable energy system, levelised cost of electricity, wind power generation, solar power generation

1. Introduction

The ambitious renewable energy targets set by European governments [1] imply that the share of renewables in electricity generation will increase significantly in the years to come. The electrification of other sectors, such as transportation, heating and cooling, will also play a major role in the transition [2, 3]. At present, the leading renewable technologies are wind, solar photovoltaics (PV) and hydroelectricity, of which only wind and solar PV have the potential for large scale expansion. For this reason, wind and solar PV are focussed upon here.

Since wind and solar PV are both Variable Renewable Energy Sources (VRES), backup generation is needed if the electrical demand is to be met at all times. Backup generation introduces additional system costs, which must be kept at a minimum.

The backup requirements depend on the mismatch between VRES generation and load. Using the degrees of freedom associated with the choice of the capacity distributions of VRES for each country, it is possible to smooth out the aggregated temporal generation pattern or even shape it towards the load pattern. As a result, the mismatch (and thus the backup requirements) is lowered. To decrease the dimensionality of the problem, renewable assets are often assigned proportional to the mean load of a country in accordance with a homogeneous wind-to-solar mixing factor. This approach is demonstrated in [4, 5], where optimal wind-to-solar mixes for Europe are found that minimise balancing and storage costs.

Further reductions in backup requirements are possible by extending the transmission network to enable more energy exchange between the countries [6, 7], but this must be balanced against the costs of transmission infrastructure. Other relevant research on the advantages and costs of grid extensions can be found in [8–12].

In this paper the assumptions of a homogeneous spatial distribution of VRES and a homogeneous wind-to-solar mixing factor are lifted and the cost-optimal siting of VRES capacities around Europe is explored.

The distribution of VRES plants is determined by at least two considerations. The first consideration is the geographical variation of the VRES quality. The resource quality is quantified through the capacity factor (CF) defined as

$$\mathrm{CF} = \frac{\text{Average generation}}{\text{Rated capacity}}. \tag{1}$$

The capacity factor is a number between 0 and 1, where 0 means no generation and 1 means maximum generation at all times. Capacity factors for the European countries for onshore wind, offshore wind and solar PV are listed in table 1.

The second consideration is the geographical variation of the temporal generation pattern for a given VRES type. This effect is particularly important for wind since Europe is large compared to the correlation length of wind [13], and wind therefore benefits from smoothing effects across the continent. Similar to the optimal wind/solar mixes

Email addresses: emilhe@phys.au.dk (Emil H. Eriksen), brown@fias.uni-frankfurt.de (Tom Brown), greiner@eng.au.dk (Martin Greiner)

found in [4, 5], optimal layouts of each VRES can be derived that, for example, reduce balancing or transmission needs.

With these points in mind, the optimal heterogeneous spatial layouts of wind and solar PV across Europe is investigated and compared to the homogeneous layouts. The main point of comparison is the average cost of electricity, which is composed of the transmission, backup and VRES costs. Different approaches to cope with the resulting large number of degrees of freedom are considered. In contrast to others who have used linear programming to optimise generation and transmission capacities simultaneously [14–16], in this paper more intuitive heuristic methods are developed to construct layouts based on knowledge of resource quality, which are then compared to layouts obtained through optimisation. For the optimisation a local search algorithm was found to be most effective given the size and non-linear formulation of the optimisation problem considered here.

This paper is organised as follows: Section 2 discusses the general modelling of the electricity system, the key metrics and the construction of heterogeneous layouts. In section 3 the performance of the different layouts and the resulting renewable penetrations for individual European countries are discussed. Section 4 contains an analysis of the sensitivity of the results to reductions in solar costs and to expansions in offshore wind capacities. We conclude the paper with a discussion on the results and an outlook on future research.

2. Methods

2.1. Renewable resource assessment

Hourly time series for the generation of onshore wind, offshore wind and solar PV for each European country were calculated using the Renewable Energy Atlas (REA). The REA time series are based on a weather data set called the Climate Forecast System Reanalysis (CFSR) from American National Centers for Environmental Prediction (NCEP) [17]. The data set covers the period from January 1979 to December 2010 and is available globally at an hourly temporal resolution and a spatial resolution of $0.31^\circ \times 0.31^\circ$.

When creating time series on a country-wise basis, the capacity factors depend strongly on the distribution of VRES in each country. While the highest capacity factor would be obtained by allocating all VRES to the best location, this is usually not possible due to space limitations and political concerns. However, since the capacity factor has a huge impact on the energy production costs, a homogeneous distribution is not realistic either. As an intermediate solution, the VRES layout was chosen as a homogeneous distribution across the 50% best grid points in each country.

For wind conversion, a multi turbine corrected power curve for the Vestas V90 3.0 MW turbine at 80 meter hub height was assumed [18]. For solar conversion, the Solar First Series 4 PV panel oriented south and tilted from horizontal to a degree equal to the latitude of installation was applied. The resulting capacity factors for each country and each technology are listed in table 1.

2.2. The electricity network

The European electricity network is modelled using a simplified 30-node model, where each node represents a country (see figure 7 for the layout of the network). The nodal load is determined from historical data, while wind and solar generation data are calculated using a combination of weather data and physical models [18]. Initially, wind is assumed to be onshore only. For each node n the generation from VRES,

$$G_n^R(t) = G_n^W(t) + G_n^S(t), \tag{2}$$

can be expressed through two parameters. The penetration γ determines the amount of energy generated relative to the mean load of the node,

$$\langle G_n^R \rangle = \gamma_n \langle L_n \rangle, \tag{3}$$

while the mixing parameter α fixes wind-to-solar ratio,

$$\langle G_n^W \rangle = \alpha_n \langle G_n^R \rangle, \tag{4}$$

$$\langle G_n^S \rangle = (1 - \alpha_n) \langle G_n^R \rangle. \tag{5}$$

The nodal difference between VRES generation and load

$$\Delta_n(t) = G_n^R(t) - L_n(t) \tag{6}$$

is called the mismatch. To avoid power outages, the demand must be met at all times. Since storage is not considered, any power deficits must be covered by backup generation. Dispatchable resources are not modelled explicitly, but are considered a part of the backup generation. If $\Delta_n(t) \geq 0$, excess energy must be curtailed $C_n(t)$, while if $\Delta_n(t) < 0$ backup generation $G_n^B(t)$ is needed. Together the two terms form the nodal balancing $B_n(t) = C_n(t) - G_n^B(t)$. It is possible to lower the balancing needs with transmission. Nodes with excess generation export energy $E_n(t)$, allowing nodes with an energy deficit to import energy $I_n(t)$ to (partly) cover their energy deficit. The nodal injection, $E_n(t) - I_n(t)$, is denoted $P_n(t)$. This leads to the nodal balancing equation,

$$G_n^R(t) - L_n(t) = B_n(t) + P_n(t), \tag{7}$$

The vector of nodal injections $\mathbf{P}$ is called the injection pattern. The actual imports and exports, and thus the injection pattern, depend on the dispatch of the nodal balancing. It is convenient to express the dispatch rules in terms of a two step optimisation problem. The top priority is to minimise the backup generation for each time step,

Table 1: Capacity factors CF_n^w, $\mathrm{CF}_n^{\tilde{w}}$ and CF_n^s for onshore wind, offshore wind and solar PV for the European countries.

	$\mathbf{CF}_n^w$	$\mathbf{CF}_n^{\tilde{w}}$	$\mathbf{CF}_n^s$		$\mathbf{CF}_n^w$	$\mathbf{CF}_n^{\tilde{w}}$	$\mathbf{CF}_n^s$		$\mathbf{CF}_n^w$	$\mathbf{CF}_n^{\tilde{w}}$	$\mathbf{CF}_n^s$
AT	0.13	-	0.16	DE	0.20	0.44	0.14	NO	0.25	0.36	0.13
BE	0.22	0.40	0.14	GB	0.32	0.44	0.13	PL	0.17	0.34	0.14
BA	0.13	-	0.18	GR	0.14	0.34	0.19	PT	0.18	0.20	0.20
BG	0.12	0.19	0.18	HU	0.12	-	0.17	RO	0.11	0.24	0.18
HR	0.17	0.23	0.18	IE	0.35	0.38	0.11	RS	0.09	-	0.18
CZ	0.15	-	0.16	IT	0.13	0.17	0.19	SK	0.12	-	0.16
DK	0.37	0.45	0.13	LV	0.23	0.34	0.13	SI	0.07	-	0.16
EE	0.26	0.32	0.13	LT	0.20	0.32	0.13	ES	0.15	0.21	0.20
FI	0.18	0.33	0.11	LU	0.19	-	0.14	SE	0.21	0.32	0.13
FR	0.20	0.34	0.17	NL	0.27	0.43	0.13	CH	0.13	-	0.18

$$\begin{aligned} \text{Step 1:} \quad & \min_{\mathbf{P},\mathbf{F}} \quad \sum_n \frac{(B_n(t))^2}{\langle L_n \rangle} \\ & \text{s.t.} \quad \sum_n P_n(t) = 0 \\ & \text{s.t.} \quad F_l^- \leq F_l(t) \leq F_l^+ \end{aligned} \tag{8}$$

where F_l is the flow on link l and $F_l^{\pm}$ denote flow constraints. By minimising B_n^2 (divided by $\langle L_n \rangle$) rather than G_n^B, the particular solution where all nodes are curtailing/generating backup synchronously (relative to $\langle L_n \rangle$) is obtained [19]. To ensure that the resulting flow obeys the physical flow equations, the objective in the second step is chosen to minimise the sum of squared flows [20].

$$\begin{aligned} \text{Step 2:} \quad & \min_{\mathbf{F}} \quad \sum_l F_l(t)^2 \\ & \text{s.t.} \quad \mathbf{P}(t) = \mathbf{P}^*(t) \\ & \text{s.t.} \quad F_l^- \leq F_l(t) \leq F_l^+ \end{aligned} \tag{9}$$

where $\mathbf{P}^*$ is the injection pattern found in step 1.

2.3. Key metrics

Following [21], the energy system cost is calculated based on a few key parameters. Besides the cost of the VRES capacities, $\mathcal{K}^{\mathcal{W}}$ and $\mathcal{K}^{\mathcal{S}}$, costs for the backup system and the transmission network are included. The backup system cost is split into two components, the cost of backup capacity $\mathcal{K}^B$ and the cost of backup energy E^B. The backup capacity cost covers expenses related to construction and to keeping the power plants online while the backup energy cost accounts for actual fuel costs. Expressed in units of the average annual load, the backup energy is given by

$$E^B = \frac{\sum_n \sum_t G_n^B(t)}{\sum_m \sum_t L_m(t)} = \sum_n \frac{\langle G_n^B \rangle}{\langle L_n \rangle}. \tag{10}$$

In principle, the backup capacity is fixed by a single extreme event. However with this definition, the results will be highly coupled to the particular data set used. To decrease the coupling, the 99% quantile is used rather than the maximum value,

$$q_n = \int_0^{K_n^B} p_n(G_n^B) dG_n^B, \tag{11}$$

where $p_n(G_n^B)$ is the time sampled distribution of backup generation and $q_n = 0.99$. With this choice, the backup system will be able to cover the demand 99% of the time. The remaining 1% is assumed to be covered by unmodelled balancing initiatives, e.g. demand side management. Given the nodal values $\mathcal{K}_n^B$, the overall backup capacity

$$\mathcal{K}^B = \sum_n \mathcal{K}_n^B \tag{12}$$

is calculated by summation. In analogy, the transmission capacity $\mathcal{K}_l^T$ is defined so that the flow is met 99% of the time. Transmission can be positive and negative, but since links are assumed bidirectional, only the magnitude (not the sign) of the flow is to be considered. Hence

$$q_l = \int_0^{K_l^T} p_l(|F_l|) dF_l, \tag{13}$$

where $p_l(|F_l|)$ is the time sampled distribution of absolute flows and $q_l = 0.99$. Since the link length varies, $\mathcal{K}^T$ is not calculated directly by summation, but instead as a weighted sum,

$$\mathcal{K}^T = \sum_l \mathcal{K}_l^T d_l, \tag{14}$$

where d_l denotes the length of link l.

In this paper E^B will be expressed in units of average annual load, $\mathcal{K}^B$ in units of average hourly load and $\mathcal{K}^T$ in units of average hourly load $\times$ megametre.

2.4. Cost modelling

Cost assumptions for the elements of an electricity system vary greatly across the literature [21]. In this study, the cost assumptions published by [22] have been adapted with a single modification. The cost of solar has been reduced by 50% in accordance with near future solar PV panel price projections [23]. The resulting estimates are listed in table 2. In general, the cost assumptions are in the low

end for VRES which reflects the expectation that the cost of VRES will go down in the future as the penetration increases [24]. Backup generation is priced based on the cost of Combined Cycle Gas Turbines (CCGTs).

Table 2: Cost assumptions for different assets separated into capital expenditures (CapEx) and fixed/variable operational expenditures (OpEx).

Asset	**CapEx** [€/W]	**OpEx$_{\text{fixed}}$** [€/kW/y]	**OpEx$_{\text{variable}}$** [€/MWh]
CCGT	0.90	4.5	56.0
Solar PV	0.75	8.5	0.0
Offshore wind	2.00	55.0	0.0
Onshore wind	1.00	15.0	0.0

From the VRES penetration, the mixing factor and the mean load, the effective generation of each node can be calculated. Dividing by the associated capacity factor, the capacity is obtained. Except for transmission capacity, the present value of each element can be calculated directly as

$$V = \text{CapEx} + \sum_t \frac{\text{OpEx}_t}{(1+r)^t} \tag{15}$$

where r is the rate of return assumed to be 4% per year. The transmission capacity cannot be translated directly into cost as the cost depends on the length and the type of the link. Link lengths have been estimated as the distance between the country capitals. Link costs are assumed to be 400€ per km per MW for AC links and 1,500€ per km per MW for HVDC links. For HVDC links, an additional cost of 150,000€ per MW per converter station pair (one at each end) is added [9, 10, 25]. The layout of AC and HVDC links has been constructed by [6] from ENTSO-E data and is shown in figure 7.

To allow for comparison of different energy systems, the Levelised Cost of Electricity (LCOE) is a convenient measure. The LCOE is the cost that every unit of energy produced during the lifetime of the project must have to match the present value of investment [26],

$$\text{LCOE} = \frac{V}{\sum_t \frac{L_{EU,t}}{(1+r)^t}}. \tag{16}$$

Since the life time of the system elements differs, the LCOE is evaluated separately for each system element. The LCOE for the complete system is calculation by summation. Life times of 25 years for solar PV and onshore wind, 20 years for offshore wind, 30 years for CCGT plants and 40 years for transmission infrastructure were assumed. See [21] for more details on the cost calculation.

2.5. Heuristic β layouts

The simplest way to distribute the renewable resources would be to assign the resources homogeneously (relative to the mean load of the node) so that $\gamma_n = \gamma_{EU}$ and $\alpha_n = \alpha_{EU}$. However this assignment might not be ideal since the capacity factors vary significantly between the nodes. Having this point in mind, an intuitive way to proceed would be to assign resources proportional to the CF. To generalise the idea, the CF is raised to an exponent β [22]. For a wind only layout, the nodal γ values are given by

$$\gamma_n^W = \gamma_{EU} \left(\text{CF}_n^W\right)^\beta \frac{\langle L_{EU}\rangle}{\sum_m \langle L_m\rangle \left(\text{CF}_m^W\right)^\beta} \tag{17}$$

where γ_{EU} is the overall penetration assumed to be 1. An equivalent expression for the solar only layout is obtained by the substitution $W \to S$. Examples for $\beta = 1$ are shown in figure 1 for the wind and solar only layouts. In the layout illustrations, each bar represents a country n. The height of the bar is γ_n while the mix α_n between onshore wind (blue) and solar (yellow) is expressed through the bar colouring. β layouts for any value of α can be constructed as a linear combination of the wind and solar only layouts with

$$\gamma_n = \alpha_{EU}\gamma_n^W + (1-\alpha_{EU})\gamma_n^S \tag{18}$$

and

$$\alpha_n = \frac{\alpha_{EU}\gamma_n^W}{\alpha_{EU}\gamma_n^W + (1-\alpha_{EU})\gamma_n^S}. \tag{19}$$

For practical reasons, it is not possible to realise extremely heterogeneous layouts. On the one hand the geographical potentials for VRES installations in countries with good renewable resources may be a limiting factor; on the other hand countries with poor renewable resources may not want to become too dependent on imports. To constrain heterogeneity, the heterogeneity factor K is introduced by requiring

$$\frac{1}{\text{K}} \leq \gamma_n \leq \text{K}. \tag{20}$$

With this definition, $\text{K} = 1$ corresponds to a homogeneous layout while $\text{K} = \infty$ represents unconstrained heterogeneity. For the β layouts, each value of K translates into an α dependent value of β. For a given value of α, the corresponding β value is found by increasing β until some country violates equation (20). At the optimal mix ($\alpha = 0.84$) $K = 1, 2, 3$ correspond to $\beta = 0.00, 0.93, 1.58$.

2.6. Heuristic CF layouts

Although the overall capacity factor of a β layout for $\beta > 0$ is higher than the capacity factor of the homogeneous layout, it is possible to achieve an even higher capacity factor without violating the constraints in equation (20). In the wind/solar PV only cases, the capacity factor is maximised by assigning $\gamma_n = \text{K}$ to the countries with the highest capacity factor for wind/solar PV and $\gamma_n = \frac{1}{\text{K}}$ to the remaining countries, except for a single in-between country which is fixed by the constraint

$$\sum_n \gamma_n \langle L_n \rangle = \langle L_{EU} \rangle. \quad (21)$$

Examples of the 'CF layout' for K = 2 are shown in figure 1. Similar to the β layouts, CF layouts for arbitrary α_{EU} values can be constructed as linear combinations of the wind and solar PV only layouts.

2.7. Optimised layouts

In this subsection the full optimisation of the layouts is considered, with the objective to minimise the LCOE with respect to the 60 variables $\gamma_1, ..., \gamma_N, \alpha_1, ..., \alpha_N$ for the $N = 30$ countries. Given the non-linear formuation of the problem in sections 2.2 and 2.3, a number of non-linear optimisation algorithms were tested including the Nelder-Mead method [27], simulated annealing [28], genetic algorithms [29] and cuckoo search [30]. It was found that the continous enforcement of the normalisation criteria equation (21) generally decreased the performance of the tested algorithms, and for that reason a new hybrid algorithm was developed to address this problem. While being a classical greedy algorithm in the sense that the locally optimal choice is always taken, the renormalisation problem was circumvented by moving only along the axial directions. The algorithm has been denoted Greedy Axial Search (GAS), and it is decribed in detail in Appendix I. All optimised layouts have been obtained using the GAS routine. These layouts will be denoted 'GAS layouts'. To decrease computation time, optimisations were performed using a one year slice of the 32 year data set. The slice was chosen as the one that statistically resembles the complete data set the most.

2.8. LCOE transmission approximation

There is a trade-off between the LCOE and the amount of transmission capacity $\mathcal{K}^T$ in the system. This trade-off is illustrated in figure 2 for the homogeneous layout at $\alpha_{EU} = 0.84$ by taking the full $\mathcal{K}^T$ and scaling it down uniformly by a factor ζ.

Because extreme events in terms of backup capacity (all countries have a large energy deficit) and transmission capacity (some countries have an energy deficit while others have excess generation) are generally not overlapping, scaling down the $\mathcal{K}^T$ initially tends to lower the LCOE since the backup capacity $\mathcal{K}^B$ is not increased accordingly.

However, if the transmission capacity is increased too far towards $\zeta = 0$, the LCOE starts to rise again, showing the benefit of a transmission grid [31]. The cost optimal value of ζ depends of the electricity system being analysed and on the specific LCOE definition (in the present case the optimum is around $\zeta = 0.5$). Obtaining the lowest possible LCOE would thus require system individual optimisation. To avoid the additional complexity associated with such an optimisation and to define the LCOE function in a consistent way, the LCOE will consistently be calculated using the synchronised export scheme at $\zeta = 1$, but with only 50% of the $\mathcal{K}^T$ cost. The approximation is shown as a dashed line in figure 2. While the transmission approximation is not perfect, the inaccuracy associated with the approximation is small compared to the uncertainty of the cost estimates. The inaccuracy is quantified in the next section.

3. Results

3.1. Dependence of results on wind-solar mix

An overview of the key parameters for each of the capacity layouts with varying α_{EU} and fixed $\gamma_{EU} = 1$ is shown in figure 3. For backup energy and backup capacity, the optimal mix is around $\alpha_{EU} = 0.9$, which is slightly higher than the values found by [4, 5]. The difference can be attributed to differences between the REA data used in this paper and the Fraunhofer-Institut für Windenergie und Energiesystemtechnik (IWES) (former ISET) data [32] used by [4, 5]. For transmission capacity, the curves are quite similar for the β layouts with a minimum around $\alpha_{EU} = 0.5$. For the CF layouts a larger increase in $\mathcal{K}^T$ is observed as K is increased. This observation is in qualitative agreement with intuition since the CF layouts are generally more extreme than the β layouts.

The main parameter of interest, the LCOE, has a maximum at $\alpha_{EU} = 0$. For the β and CF layouts it drops steadily as α_{EU} is increased until around $\alpha_{EU} = 0.84$ where the minimum is located. The GAS optimised layouts are also to be found in the wind dominated region, but their α values are generally lower. The high cost at $\alpha_{EU} = 0$ is caused by a combination of high backup energy/capacity costs and the fact that the CF of solar is generally lower than for onshore wind. The cost of producing one unit of energy is thus higher for solar than for onshore wind even though the CapEx is lower for solar.

3.2. Cost comparison of different layouts

The componentwise costs for the α-optimal β, CF and GAS layouts are given in table 3 and graphed in figure 4. If the total LCOE is considered, there is a clear trend of cost reduction as the heterogeneity parameter K is increased, allowing sites with better capacity factors to be exploited. For each value of K the cost is also reduced as the layout is optimised further from the β to the CF to the GAS layout. At $K = 1$ the LCOE sinks by 9% from the homogeneous layout at 68.2€/MWh to 62.2€/MWh in the GAS layout. At $K = 3$ there is more freedom for the GAS algorithm to optimise the heterogeneous layout and the cost drops 11% from 63.9€/MWh in the β layout to 56.9€/MWh in the GAS layout.

With regard to the costs of each component of the LCOE, the transmission costs are higher in the GAS layout than the heuristic layouts due to the more heterogenous distribution of VRES, but this is more than offset by the reduction in VRES costs, which dominate the total costs. The reduction in VRES costs is a direct result of the improved

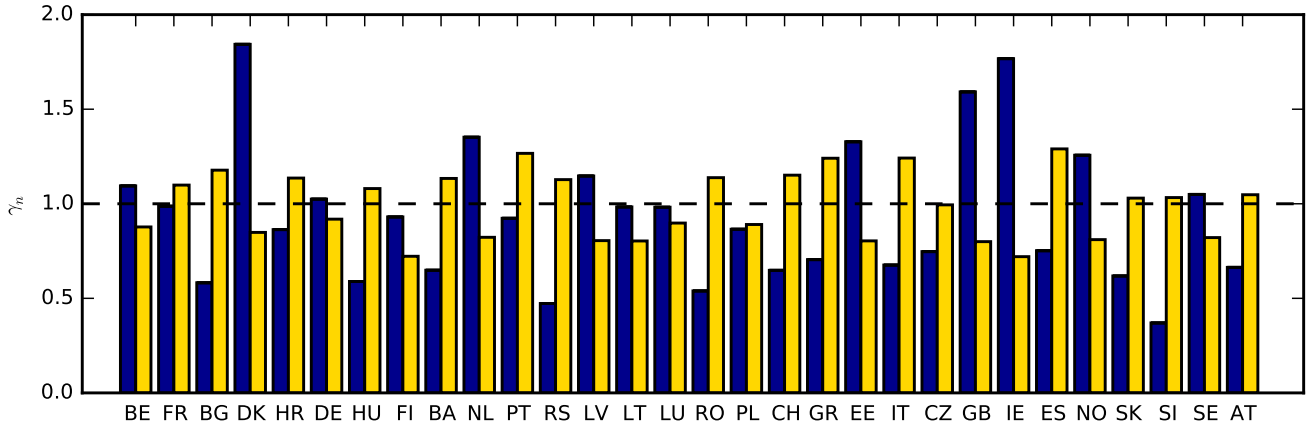

(a) Examples of β layouts for $\beta = 1$.

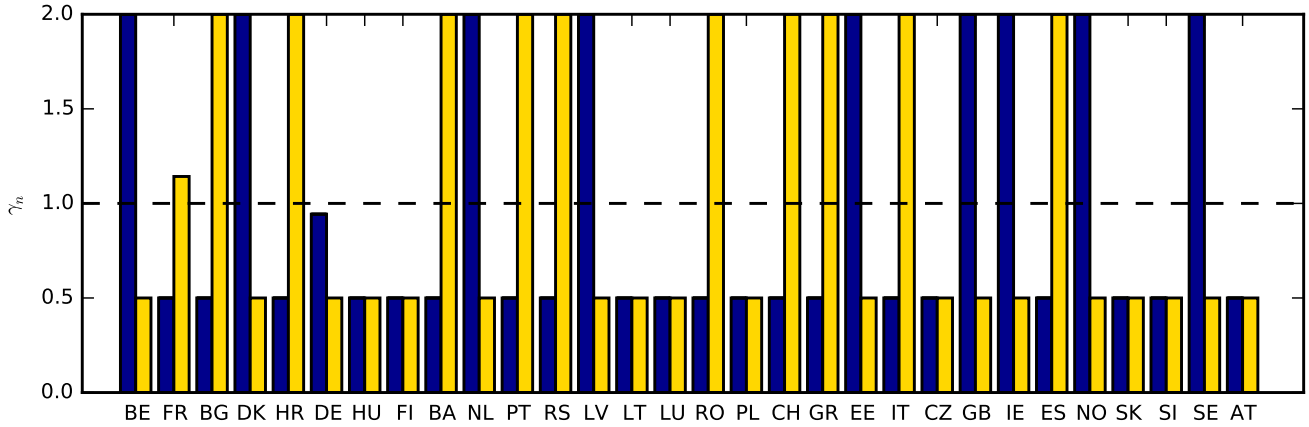

(b) Examples of CF layouts constrained by K = 2 .

Figure 1: Examples of heuristic layouts. In each sub figure, two sets of bars are shown corresponding to the $\alpha_{EU} = 1$ and 0 layouts.

Table 3: Componentwise LCOE for the optimal β, CF and GAS layouts along with the homogeneous layout without transmission. The K values are expressed through the index notation, e.g. $K = i$ for β_i. All costs are listed in €/MWh.

Parameter	**No transmission**	$\boldsymbol{\beta_1}$	$\mathbf{CF_1}$	$\mathbf{GAS_1}$	$\boldsymbol{\beta_2}$	$\mathbf{CF_2}$	$\mathbf{GAS_2}$	$\boldsymbol{\beta_3}$	$\mathbf{CF_3}$	$\mathbf{GAS_3}$
$\mathcal{K}^W$	42.79	42.79	42.79	29.80	39.83	36.52	29.20	38.18	32.79	28.53
$\mathcal{K}^S$	6.91	6.91	6.91	10.59	6.75	6.25	8.24	6.66	5.92	6.72
$\mathcal{K}^B$	6.92	4.88	4.88	5.40	4.89	4.93	5.19	4.91	5.00	5.11
E^B	16.70	10.69	10.69	12.94	10.68	10.71	11.54	10.71	10.84	10.89
$\mathcal{K}^T$	0.00	2.95	2.95	3.43	3.12	4.09	4.54	3.42	5.26	5.65
Total	73.32	68.22	68.22	62.16	65.27	62.50	58.71	63.88	59.81	56.90

average capacity factors in the GAS layout, which allow the same energy yield for lower overall capacity. Compared to the transmission and VRES costs, the backup costs remain relatively constant.

One reason that the GAS optimisation might have been better than the heuristic layouts is that the GAS algorithm sees not just the capacity factors at each site, like the heuristic layouts, but also the geographical variation of the temporal generation pattern, which the GAS algorithm can exploit to shape the VRES generation pattern to the load. However if this was the reason, the backup generation costs would have decreased from the heuristic to the GAS layout, which they do not; in fact the backup costs rise very slightly. This suggests that the GAS optimisation's success really lies with the freer exploitation of capacity factors.

Compared to the β and CF layouts, the GAS layouts include a slightly larger solar component. The magnitude of the solar component for the GAS layouts drops with increasing K value. As the heterogeneity constraints are

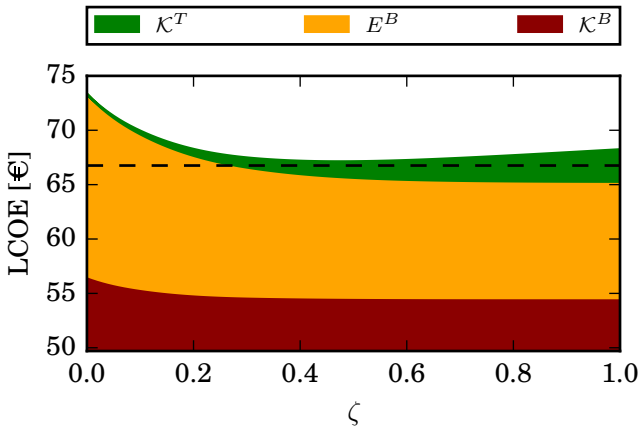

Figure 2: Non-VRES components of the LCOE for different values of ζ. The constant VRES part (omitted) consists of 42.8€/MWh for wind and 6.9€/MWh for solar. The dashed line indicates the approximated LCOE (see text). The calculations were performed using a homogeneous layout with $\alpha_{EU} = 0.84$ (cost optimal mix) and the synchronised export scheme.

loosened wind becomes more favourable since it becomes possible to allocate more resources to the sites with a very high CF. A similar effect is present for solar, but it is less dominant since the difference between the higest and lowest CF for solar (0.20, Spain vs. 0.11, Finland) is much smaller than for wind (0.37, Denmark vs. 0.07, Slovenia).

3.3. Distribution of capacity layouts

In this section the geographical distribution of wind and solar capacities is examined. The β and CF layouts for $K = 2$ are compared to the homogeneous layout in figure 5 while the GAS layouts for $K = 1, 2, 3$ are shown in figure 6. From the two heuristic layouts shown in figure 5 it is clear that the CF layout achieves a much greater degree of heterogeneity than the β layout, whose heterogeneity is limited by the first country to hit the $K = 2$ boundary (in this case Slovenia at $\gamma_n = 1/2$). This is reflected in the CF layout's lower LCOE. In fact the CF layout is not far from the GAS layout for $K = 2$ in figure 6: in both layouts there is a predominance of wind in Denmark, the Netherlands, Great Britain, Ireland and Norway.
As the heterogeneity parameter K is increased for the GAS layouts, wind dominates in terms of energy. At $K = 2$ and $K = 3$ it is interesting to note that all the countries are either completely solar or completely wind dominated (with the only exception of Lithuania for $K = 3$, which is mostly wind). This choice appears to be entirely correlated with which VRES technology has the higher capacity factor in each country (see table 1 for the capacity factors; the only exception is Croatia, where the capacity factors are anyway very close together). This confirms that the GAS algorithm is largely optimising by capacity factor.

3.4. Transmission capacities

As seen in figure 4, the cost of transmission increases with increasing heterogeneity. To quantify what happens, the link usage for the homogeneous layout and the GAS layout for K = 2 is visualised in figure 7. Comparing figure 7a and figure 7b it is clear that the flow does not increase homogeneously across the network. The primary increase is on links connecting countries with severe excess generation, e.g. Great Britain, Ireland, the Netherlands, Norway and Denmark. However, additional flows are also induced on links connected to Germany and France, which act as transit countries. The capacity of links connecting south and central European countries remains practically unchanged.

3.5. Validity of transmission approximation

To assess the validity of the LCOE transmission approximation proposed in section 2.8, the value of ζ was optimised to minimise the LCOE for the values of γ_n, α_n in the GAS layout for each value of K. The results are plotted in figure 3 as hexagons, where the optimised values of ζ are 0.43, 0.44 and 0.45 for K = 1, 2 and 3 respectively.
From the comparison it is clear that the approximation generally works well. The LCOE is underestimated slightly, and the error tends to increase with K. At $K = 2$ the approximated LCOE is off by 1.3%.

4. Sensitivity analysis

4.1. Reduced solar cost

For the β as well as the CF layouts, the optimal mix is around $\alpha_{EU} = 0.84$. As mentioned previously, wind domination is partly a consequence of the higher cost of energy generation for solar PV compared to onshore wind. The cost of solar has dropped rapidly in the recent years and this tendency might very well continue. To shed some light on the consequences of further price reductions, the sensitivity of the optimal mix to reductions in the solar cost has been examined. Figure 8 illustrates the change in LCOE for the GAS optimised layouts when the solar cost is reduced by 25%, 50% and 75% respectively. The 0% scenario is included as a reference.
A reduction of the solar cost by 25% does not change the picture much. The optimal mix is shifted from above 0.75 to below 0.75 and the LCOE drops by around 2€ (cost comparison numbers are calculated for the GAS layouts at K = 2). As the solar cost is reduced by 50% the cost at $\alpha_{EU} = 0$ (pure solar) becomes comparable to the cost at $\alpha_{EU} = 1$ (pure wind). The optimal mix drops to around 0.6 and the LCOE is reduced by almost 6€ compared to the reference scenario. Reducing the cost of solar by 75%, solar becomes much cheaper than wind, and the optimal mix is shifted below $\alpha_{EU} = 0.5$ indicating solar domination. Compared to the reference scenario, the LCOE dropped by more than 10€. However, it should be noted that such large cost reductions for PV may not be plausible: much of the recent cost reduction has come from

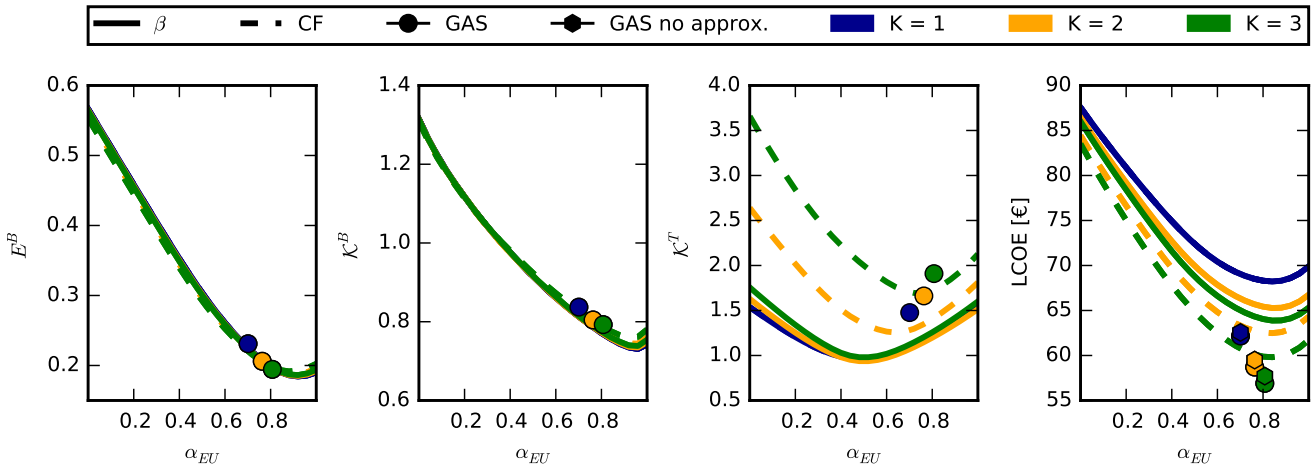

Figure 3: Overview of the key parameters and the associated LCOE as a function of α_{EU}. The β and CF layouts are shown as solid and dashed lines respectively. The GAS layouts are plotted as dots. Different constraints are shown: K = 1 (blue), 2 (yellow) and 3 (green).

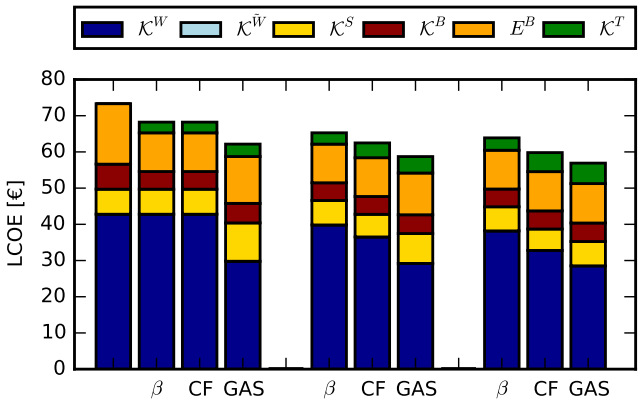

Figure 4: Componentwise LCOE for the optimal β, CF and GAS layouts for K = 1 (left), 2 (middle) and 3 (right). The unlabelled bar represents the homogeneous layout without transmission.

reduced material costs; the remaining costs come from the installation, where it is not so easy to economise.

4.2. Offshore wind

So far, wind has been assumed to be onshore only. By January 2014, the total European onshore wind capacity was 120.8GW, while the offshore capacity was 8.0GW [33]. The increasing share of offshore wind raises the question, how the LCOE will be affected by the introduction of an offshore component. The immediate expectation would be a significant increase in the LCOE, since the expenditures for offshore wind are more than 100% higher than for onshore wind due to foundation expenses and increased maintenance costs. On the other hand the capacity factors for offshore sites are generally higher than for onshore sites.

It would be possible to introduce offshore wind on equal footing with onshore wind and solar PV. However, since offshore wind is much more expensive, an optimised layout would pose a 0% offshore component, which is not an interesting nor surprising result. Instead, a fixed offshore component is introduced by splitting the wind component into an onshore γ^W and an offshore $\gamma^{\tilde{W}}$ component,

$$\gamma^W \rightarrow \gamma^{\mathrm{W}} + \gamma^{\tilde{W}}, \tag{22}$$

for countries with suitable offshore regions. In practice these are the North Sea countries (Denmark, Germany, Great Britain, Ireland, the Netherlands, France, Belgium, Norway and Sweden). Other countries retain onshore wind only. The magnitude of the offshore component is defined by requiring that the offshore wind power generation accounts for a fixed share of the total wind power generation. Cost details for optimised layouts with fixed offshore shares of 25% and 50% are shown in figure 10. The 0% scenario is included as a reference.

From figure 10 it is clear that the introduction of an offshore component increases the LCOE. However, the increase in LCOE is not dramatic. While the cost of wind increases significantly, the cost of backup and transmission decreases slightly. The decrease is a consequence of the difference in the temporal generation pattern from onshore to offshore wind. In some time steps the onshore generation is low while the offshore generation is high. The introduction of an offshore component thus tends to smooth out the wind generation time series. The GAS optimised layouts for an offshore share of 50% are shown in figure 11.

5. Discussion and conclusions

The cost-optimal distribution of VRES around Europe has been investigated for the case where the mean VRES generation equals the mean load ($\gamma_{EU} = 1$). It was found that although the costs of backup generation and transmission are significant, the main costs are associated with the

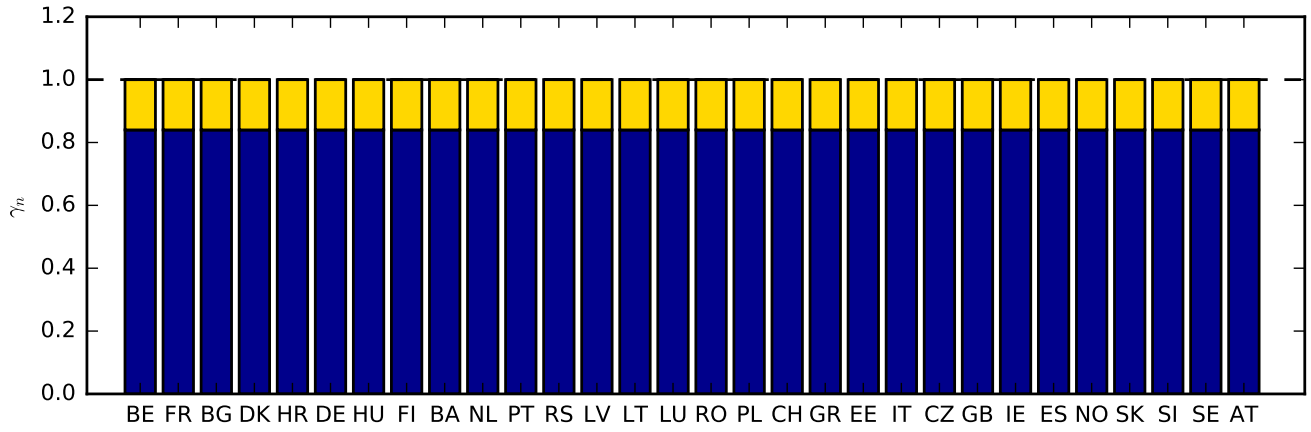

(a) Homogeneous layout.

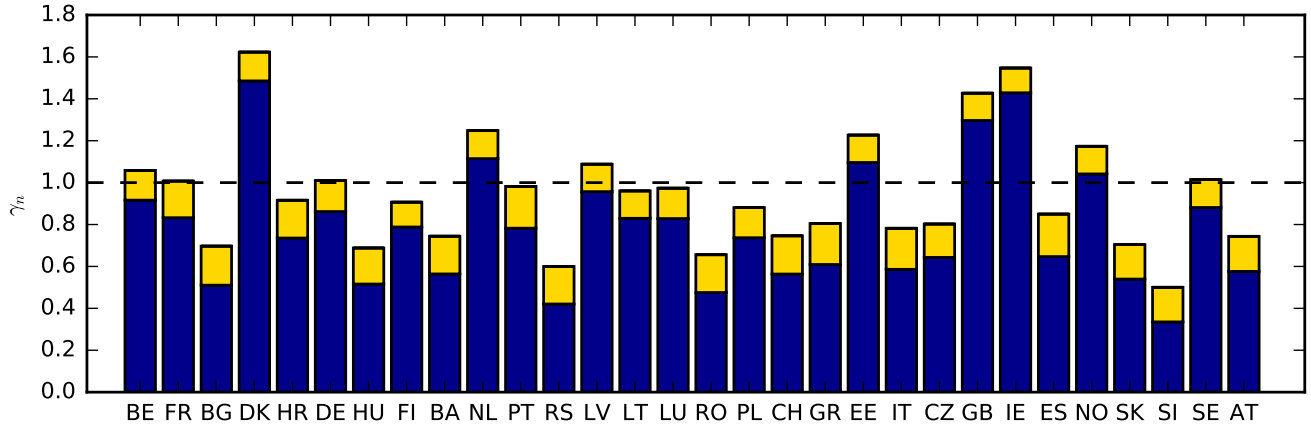

(b) β layout constrained by $K = 2$.

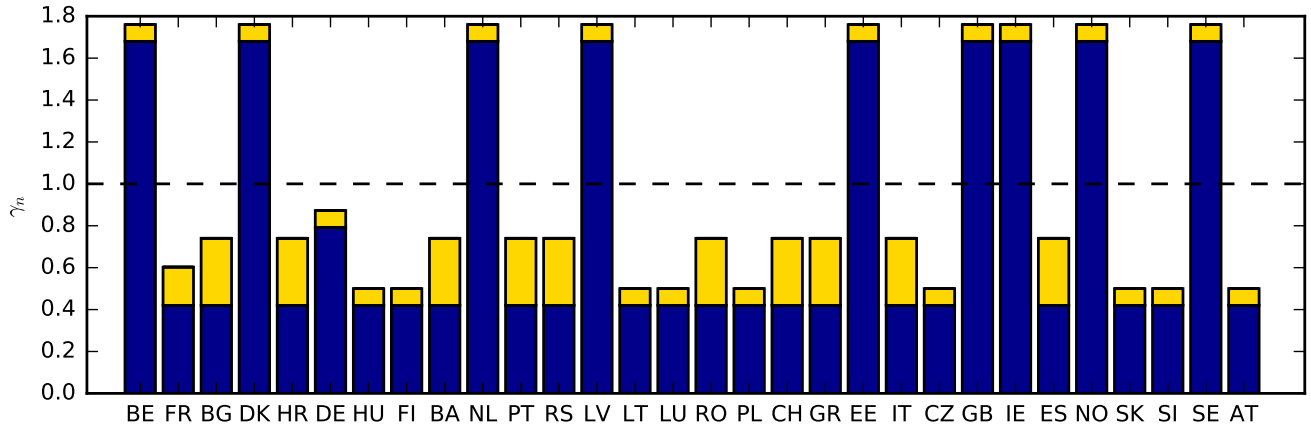

(c) CF layout constrained by $K = 2$.

Figure 5: Comparison of the homogeneous layout (a) with the β and CF layouts constrained by $K = 2$ (b, c).

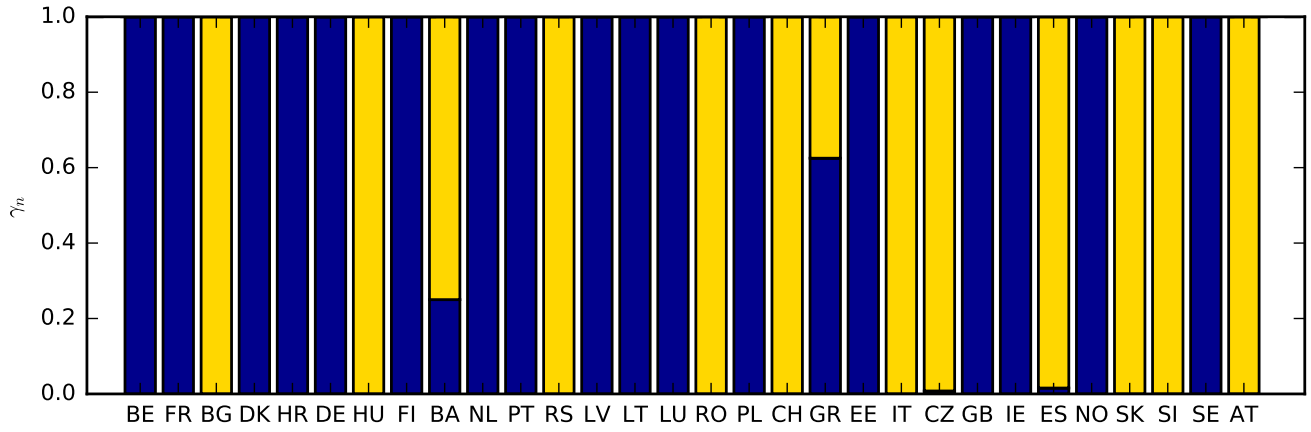

(a) GAS layout constrained by K = 1.

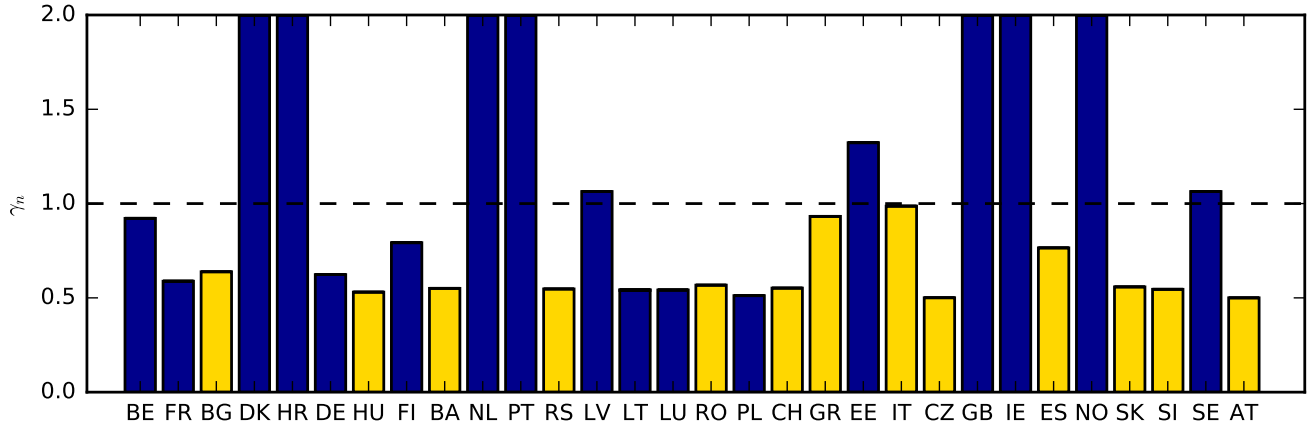

(b) GAS layout constrained by K = 2.

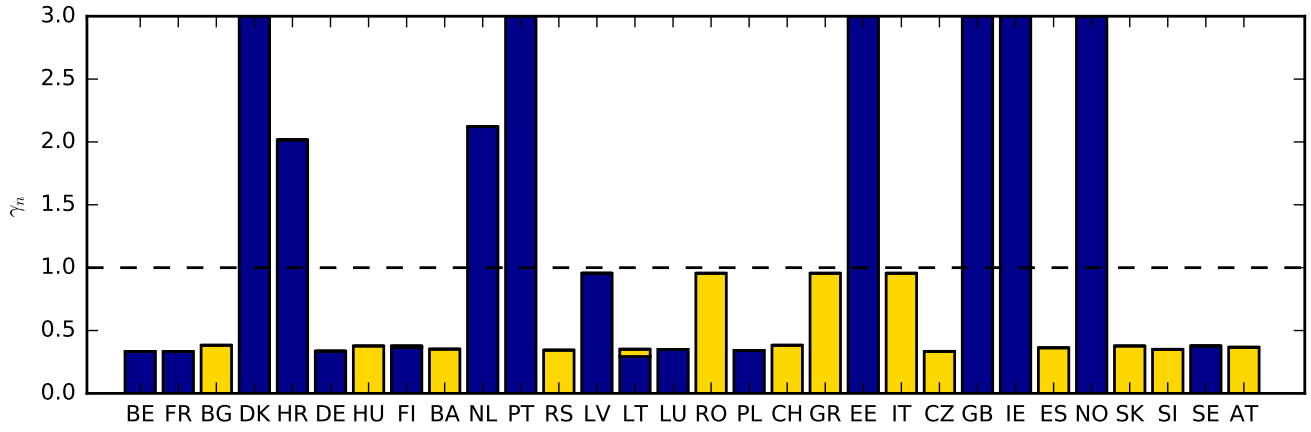

(c) GAS layout constrained by K = 3.

Figure 6: GAS optimised layouts for different k values.

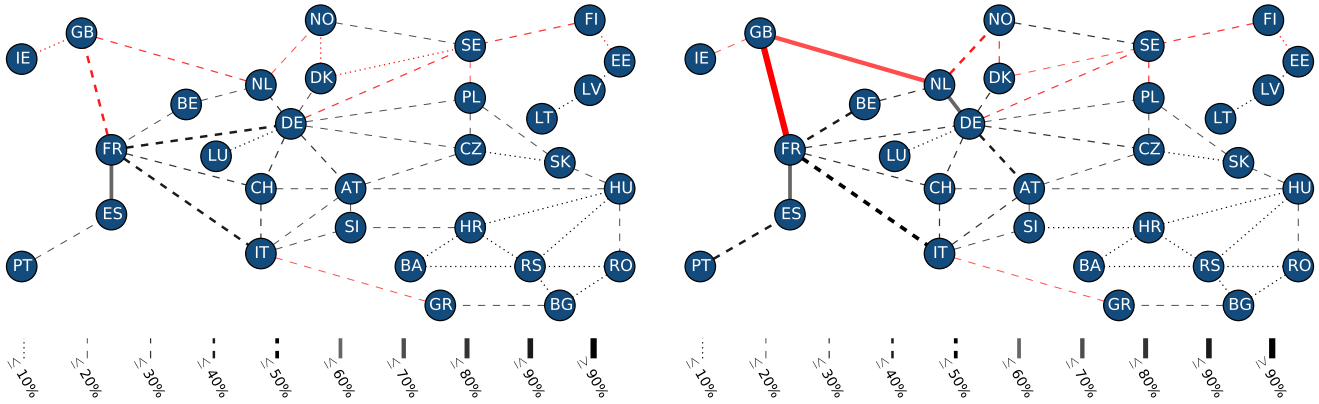

(a) Link usage for the homogeneous layout.

(b) Link usage for the GAS layout constrained by K = 2.

Figure 7: Overview of link usage. AC links are shown in black while HVDC links are shown in red. Link capacities are calculated as per equation (13) and indicated relative to the highest flow (103 GW between Great Britain and France in figure 7b).

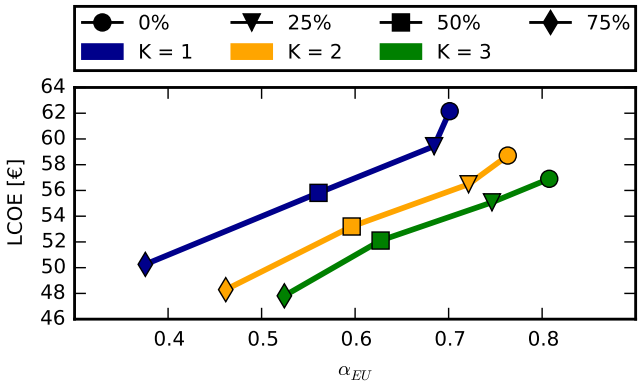

Figure 8: LCOE of the GAS optimised layouts when the solar cost is reduced by 25% (triangle), 50% (square) and 75% (diamond). The 0% scenario (circle) is included as a reference. Different constraints are shown: K = 1 (blue), 2 (yellow) and 3 (green).

VRES capacities. The VRES capacity costs can be lowered by allocating more resources to countries with high capacity factors and by preferring onshore wind over solar PV. Allowing each country to install VRES capacities covering a minimum of 50% and a maximum of 200% of their mean load, the LCOE can be lowered by more than 8% by choosing the heuristic CF layout which maximises the overall capacity factor. An additional 6% reduction of the LCOE was achieved by explicit optimisation, whose final layout was close to the heuristic CF layout based only on capacity factors. This cost reduction can be attributed to the general tendency for the heterogeneous layouts to shift wind capacities towards the North Sea countries. Since the wind resource quality is better than for the central and southern countries, this reallocation results in lower costs.
In the past onshore wind has been the predominant VRES and the cost-optimal mixes presented here are also dominated by onshore wind, based on current cost projections. However, the cost of solar PV has dropped more rapidly than expected in recent years, and solar PV has already reached grid parity in some markets [34]. If this decreasing price trajectory continues much longer, the cost optimal mix may end up around $\alpha_{EU} = 0.6$, indicating almost equal amounts of wind and solar in the energy mix.
The main analysis considered onshore wind only, but the effect of introducing an offshore component was also discussed. Although capacity factors offshore are higher than onshore and the temporal generation pattern is more stable, these advantages are offset by the higher costs arising from expensive offshore foundations and increased maintenance costs. However, offshore wind has several other benefits: the opposition from the public is usually lower than for onshore wind, and the potential for expansion larger. When feasible onshore sites have been exhausted, offshore wind might present the best alternative.
There are several avenues for further investigations. The cost assumption for the backup generation is based on the worst-case scenario that all backup is provided by gas turbines. In reality, up to 17% of Europe's electricity supply is already provided by hydroelectric plants, most of which are flexible, some of which have storage capacity and all of which produce electricity at very low marginal cost. Incorporating hydroelectricity in the modelling would reduce the LCOE further.
In addition, a full assessment of the geographical resource potentials in each country for each VRES technology would allow further heterogeneity beyond the $K = 2, 3$ limits considered here, which would also result in a lower LCOE. Similarly an increase in the spatial resolution of the model would allow more fine-tuned allocation of renewables to sites with the highest capacity factors, resulting in a yet lower LCOE.
An unequal distribution of renewable energy generation raises the question of who should pay for the generation and transmission assets. Recent work on the allocation of network flows to users in highly renewable networks [35, 36] may provide the basis for an equitable distribution of the costs of a highly heterogeneous system.

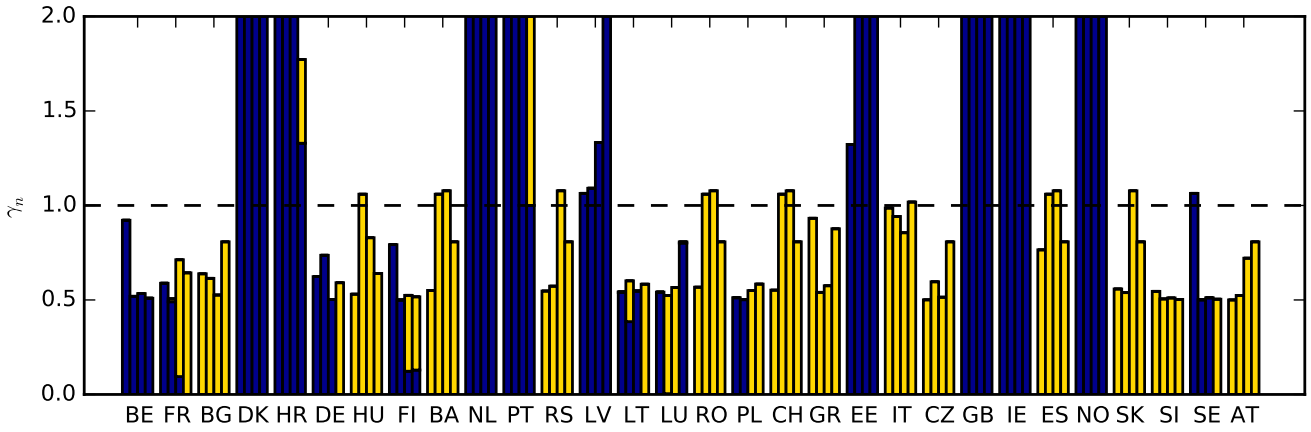

Figure 9: GAS optimised layouts constrained by K = 2 for a solar cost reduction of (from left to right) 0% (reference), 25%, 50% and 75%.

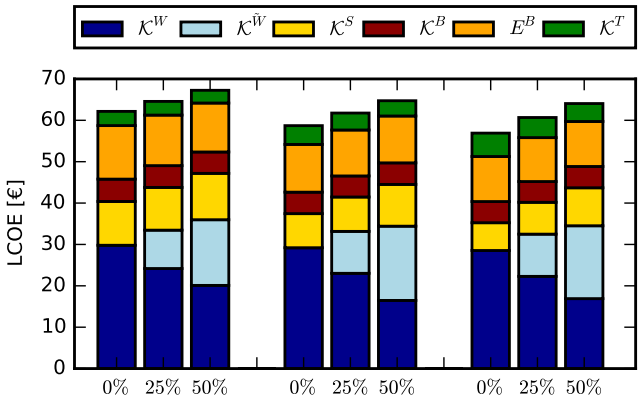

Figure 10: Cost details for the GAS optimal layouts for K = 1 (left), 2 (middle) and 3 (right) for offshore shares of 0%, 25% and 50%.

Bibliography

[1] European Commission. A roadmap for moving to a competitive low carbon economy in 2050. Technical report, EC, March 2011.

[2] James H. Williams, Andrew DeBenedictis, Rebecca Ghanadan, Amber Mahone, Jack Moore, William R. Morrow, Snuller Price, and Margaret S. Torn. The Technology Path to Deep Greenhouse Gas Emissions Cuts by 2050: The Pivotal Role of Electricity. Science, 335:53–59, 2012. http://dx.doi.org/10.1126/science.1208365.

[3] McKinsey & Company, KEMA, The Energy Futures Lab at Imperial College London, Oxford Economics, and ECF. Roadmap 2050 – A practical guide to a prosperous, low-carbon Europe. Technical report, European Climate Foundation, http://www.roadmap2050.eu/, April 2010. Online, accessed June 2012.

[4] Heide, D., von Bremen, L., Greiner, M., Hoffmann, C., Speckmann, M., and Bofinger, S. Seasonal optimal mix of wind and solar power in a future, highly renewable Europe. Renewable Energy, 35(11):2483–2489, 2010.

[5] Heide, D., Greiner, M., Von Bremen, L., and Hoffmann, C. Reduced storage and balancing needs in a fully renewable European power system with excess wind and solar power generation. Renewable Energy, 36(9):2515–2523, 2011.

[6] Rolando A. Rodriguez, Sarah Becker, Gorm Bruun Andresen, Dominik Heide, and Martin Greiner. Transmission needs across a fully renewable European power system. Renewable Energy, 63:467–476, March 2014.

[7] Sarah Becker, Rolando A. Rodríguez, Gorm B. Andresen, Stefan Schramm, and Martin Greiner. Transmission grid extensions during the build-up of a fully renewable pan-European electricity supply. Energy, 64:404–418, January 2014.

[8] Papaemmanouil, A., Tuan, L.A., Andersson, G., Bertling, L., and Johnsson, F. A cost-benefit analysis of transmission network reinforcement driven by generation capacity expansion. In Power and Energy Society General Meeting, pages 1–8. IEEE, 2010.

[9] Schaber, K., Steinke, F., and Hamacher, T. Transmission grid extensions for the integration of variable renewable energies in Europe: Who benefits where? Energy Policy, 43:123 – 135, 2012.

[10] Schaber, K., Steinke, F., Mühlich, P., and Hamacher, T. Parametric study of variable renewable energy integration in Europe: Advantages and costs of transmission grid extensions. Energy Policy, 42:498–508, 2012.

[11] Egerer, J., Lorenz, C., and Gerbaulet, C. European electricity grid infrastructure expansion in a 2050 context. In 10th International Conference on the European Energy Market, pages 1–7. IEEE, 2013.

[12] Brown, T., Schierhorn, P., Tröster, E., and Ackermann, T. Optimising the European transmission system for 77% renewable electricity by 2030. IET Renewable Power Generation, 10(1):3–9, 2016.

[13] J. Widen. Correlations between large-scale solar and wind power in a future scenario for sweden. IEEE Transactions on Sustainable Energy, 2(2):177–184, 2011.

[14] Gregor Czisch. Szenarien zur zukünftigen Stromversorgung. PhD thesis, Universität Kassel, 2005.

[15] Yvonne Scholz. Renewable energy based electricity supply at low costs - Development of the REMix model and application for Europe. PhD thesis, Universität Stuttgart, 2012.

[16] Hagspiel, S., Jägemann, C., Lindenburger, D., Brown, T., Cherevatskiy, S., and Tröster, E. Cost-optimal power system extension under flow-based market coupling. Energy, 66:654–666, 2014.

[17] Saha, S. et al. The ncep climate forecast system reanalysis. Bull. Amer. Meteor. Soc., 91(8):1015–1057, 2010.

[18] Gorm Bruun Andresen, Anders Aspegren Søndergaard, and Martin Greiner. Validation of danish wind time series from a new global renewable energy atlas for energy system analysis. Energy, 2015.

[19] Rolando A. Rodriguez, Magnus Dahl, Sarah Becker, and Martin Greiner. Localized vs. synchronized exports across a highly renewable pan-european transmission network. Energy, Sustainability and Society, 5(1), 2015.

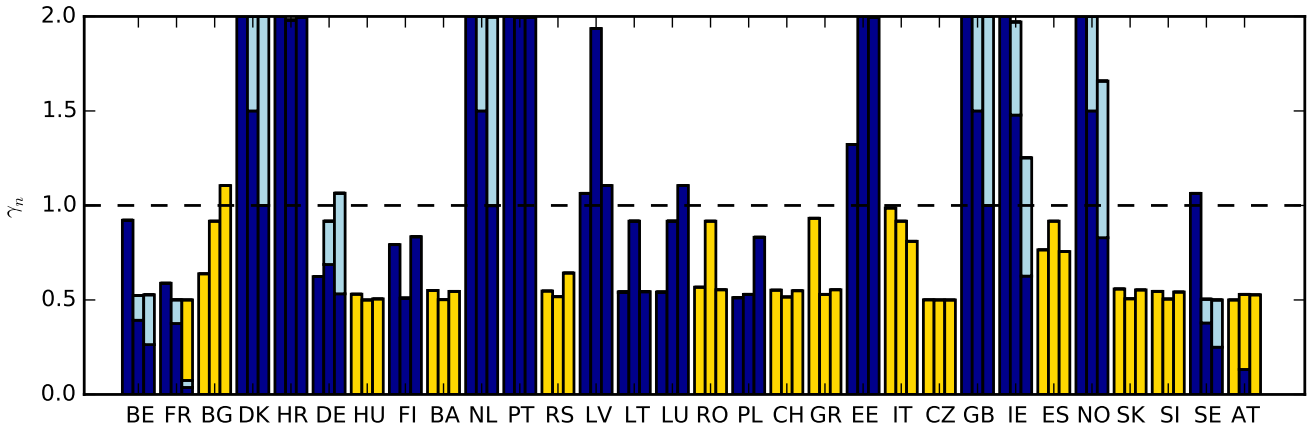

Figure 11: GAS optimised layouts constrained by K = 2 for an offshore share of (from left to right) 0% (reference), 25% and 50%.

[20] Magnus Dahl. Power-flow modeling in complex renewable electricity networks. Master's thesis, Aarhus University, 2015.

[21] Rolando A. Rodriguez, Sarah Becker, and Martin Greiner. Cost-optimal design of a simplified, highly renewable pan-european electricity system. Energy, 83:658 – 668, 2015.

[22] Rolando A. Rodriguez. Weather driven power transmission in a highly renewable European electricity network. PhD thesis, Aarhus University, 2014.

[23] Zuzana Dobrotkova, Al Goodrich, Miller Mackay, Cedric Philibert, Giorgio Simbolotti, and Professor XI Wenhua. Renewable energy technologies: Cost analysis series, solar photovoltaics. Technical Report 4/5, The International Renewable Energy Agency, 2012.

[24] Kost, C., Schlegl, T., Thomsen, J., Nold, S., and Mayer, J. Levelized cost of electricity: renewable energies. Technical report, Fraunhofer Institute for solar energy systems ISE, 2012. Online, retrieved October 2013.

[25] McKinsey. RoadMap 2050: A Practical Guide to a Prosperous, Low-Carbon Europe. Technical report, European Climate Foundation, 2010. Online, retrieved October 2013.

[26] W. Short, D. Packey, and T. Holt. A manual for the economic evalua- tion of energy efficiency and renewable energy technologies. Technical report, National Renewable Energy Laboratory, 1995.

[27] J. A. Nelder and R. Mead. A simplex method for function minimization. The Computer Journal, 7(4):308–313, 1965.

[28] S. Kirkpatrick, C. D. Gelatt, and M. P. Vecchi. Optimization by simulated annealing. Science, 220(4598):671–680, 1983.

[29] David E. Goldberg. Genetic Algorithms in Search, Optimization and Machine Learning. Addison-Wesley Longman Publishing Co., Inc., Boston, MA, USA, 1st edition, 1989.

[30] Xin-She Yang and Suash Deb. Cuckoo search via lévy flights. In NaBIC, pages 210–214. IEEE, 2009.

[31] Rodriguez, R.A., Becker, S., Andresen, G., Heide, D., and Greiner, M. Transmission needs across a fully renewable European power system. Renewable Energy, 63:467–476, 2014.

[32] Stefan Bofinger, Lüder von Bremen, Kaspar Knoor, Katharina Lesch, Kurt Rohrig, Yves-Marie Saint-Drenan, and Markus Speckmann. Raum-zeitliche erzeugungsmuster von wind- und solarenergie in der ucte-region und deren einfluss auf elektrische transportnetze. Technical report, Institut für Solare Energieversorgungstechnik, 2008.

[33] G. Corbetta, I. Pineda, and J. Wilkes. Wind in power 2014 european statistics. Technical report, The European Wind Association, 2015.

[34] Vishal Shah, Jerimiah Booream-Phelps, and Susie Min. 2014 outlook: Let the second gold rush begin. Technical report, Deutsche Bank Markets Research, 2014.

[35] Brown, T. Transmission network loading in europe with high shares of renewables. IET Renewable Power Generation, 9(1):57–65, 2016.

[36] Bo Tranberg, Anders B Thomsen, Rolando A Rodriguez, Gorm B Andresen, Mirko Schäfer, and Martin Greiner. Power flow tracing in a simplified highly renewable european electricity network. New Journal of Physics, 17, 2016.

Appendix I. Greedy Axial Search

When a solution is renormalised, all γ values are scaled either up or down. Therefore, it is possible that some γ values end up outside the boundaries. Applying the box method and doing another rescaling would normally cause an infinite loop, but if the troublesome γ values are fixed at the boundary and the rescaling is only applied to the remaining free γ values, the infinite loop is avoided. In general this approach is problematic since it can change the direction of the search. However, in one particular case, that does not matter. Consider a step up/down in γ along axis i. In this case all other γ values are scaled down/up. Keeping γ_i fixed while applying the renormalisation procedure as described above, the feasibility of moving up/down *along axis* i can be determined. This is the underlying principle of Greedy Axial Search (GAS).

As any greedy algorithm, the GAS algorithm works by taking the locally optimal choice. Hence the feasibility for each direction is evaluated, but only the best choice is accepted. This process is repeated until a convergence criteria is fulfilled. At this point the step size is reduced and the iterative optimisation procedure repeated until the step size drops below some tolerance. The algorithm structure is sketched in algorithm 1.

The *StepUp* and *StepDown* subroutines generate new solutions by stepping a solution (first argument) up/down along dimension i (second argument) with some step size (third argument) after which the solution is renormalized as described above. Compared to algorithm 1 a few tricks have been implemented to improve performance (e.g. if the step up along dimension i turned out to be favourable,

the step down solution is not evaluated). Performance tweaks were left out for clarity. Values of $maxStepSize = 1$, $minStepSize = 5 \cdot 10^{-3}$ and $tolerance = 10^{-3}$ were found to be appropriate.

Algorithm 1 Pseudo code for the greedy axial search implementation. The *Evaluate* function evaluates solution costs. By passing an array of solutions to the *Evaluate* function, rather than evaluation the solutions one by one, parallel evaluation is possible. The *Sort* function sorts the solutions by cost in ascending order.

```
function GreedyAxialSearch
    best ← solution selected randomly from within the solution space
    deltaCost ← ∞
    stepSize ← maxStepSize
    while stepSize > minStepSize do
        while deltaCost > tolerance do
            for index i = 0 to 2N do
                trailSolutions[i]← StepUp(best,i,stepSize)
                trailSolutions[i+2N]← StepDown(best,i,stepSize)
            Evaluate(trailSolutions)
            Sort(trailSolutions)
            deltaCost ← cost of best minus cost of trailSolutions[0]
            if deltaCost > 0 then
                best ← trailSolutions[0]
        stepSize ← stepSize/2
    return best
```